



Design and testing of a miniature silicon strip detector

Shen Wang^{1,2,3,4} · Wei Chen^{1,2,5} · Jian-Hua Guo^{1,2,4}

Received: 11 January 2019/Revised: 7 August 2019/Accepted: 15 October 2019/Published online: 26 December 2019
© China Science Publishing & Media Ltd. (Science Press), Shanghai Institute of Applied Physics, the Chinese Academy of Sciences, Chinese Nuclear Society and Springer Nature Singapore Pte Ltd. 2019

Abstract In this study, we developed a multi-channel low-noise electronic readout system for a silicon strip detector. Using two charge-sensitive amplifier VA140 chips from IDEAS in Norway, the system has a wide linear dynamic input range of up to 180 fC for 128 channels with 0.16 fC average equivalent noise charge. In addition, we studied the charge distribution behaviors between adjacent silicon strips with the help of transient current technology.

Keywords SSD · VA140 · TCT · Readout electronics

This work was supported by the National Natural Science Funds of China (Nos. 11622327 and U1831206), Youth Innovation Promotion Association of the Chinese Academy of Sciences (No. 2014275), and Strategic Pioneer Program on Space Science of the Chinese Academy of Sciences (No. XDA15010200).

✉ Jian-Hua Guo
jhguo@pmo.ac.cn

¹ Purple Mountain Observatory, Chinese Academy of Sciences, Nanjing 210023, China

² Key Laboratory of Dark Matter and Space Astronomy, Chinese Academy of Sciences, Nanjing 210023, China

³ School of Astronomy and Space Science, University of Science and Technology of China, Nanjing 210023, China

⁴ University of Science and Technology of China, Hefei 230026, China

⁵ University of Chinese Academy of Science, Beijing 100049, China

1 Introduction

Silicon strip detectors (SSDs) are widely used as tracker or vertex detectors in high-energy physics experiments [1–4]. Spatial resolution is the most important parameter of SSDs. For example, SSDs with a 25 μm strip pitch can provide a spatial resolution greater than 1.25 μm [5]. Simultaneously, the ionization energy of silicon is approximately 3.6 eV, which is much smaller than in a gas detector or in scintillation crystals. Accordingly, SSDs have a high energy resolution capability.

With the development of high-energy physics experiments in China, SSDs are expected to have much wider application prospects. The dark matter particle explorer (DAMPE) [6] satellite utilizes 12 layers of a single-sided SSDs as a tracker detector. This tracker detector has the capacity to measure the electrical charge of incoming cosmic rays and the direction of incident photons. For future Chinese large collider experiments that use a circular electron positron collider (CEPC) [7], applying SSDs in both barrel and forward/backward regions as components of the tracking system has been proposed.

In this study, we designed a miniature SSD readout system and discuss its linear response, noise performance, charge-sharing effect, and cosmic ray spectrum. In Sect. 2, we present a detector system that includes both front-end and data acquisition (DAQ) parts. Section 3 of this paper briefly reports on transient current technology (TCT) [8], which we used to test linearity and to study charge sharing. Section 4 presents experimental results on linearity and noise performance and introduces an η algorithm to study charge distribution behaviors between detector strips. Section 4 also presents the cosmic ray spectrum measured by the SSD system.

2 Detector system

The detector system consists of one DAQ board and one front-end electronics board on which the silicon detectors are mounted, as shown in Fig. 1. A software for this multi-channel detector system operation and data acquisition was developed [9].

When the detector system is running, a reversed bias for full depletion is applied on the silicon strip p-n junction. Once a charged particle passes through the detector, a charge signal is induced on the detector electrode. This signal is collected and processed by the electronic system. With further analysis, we can determine the deposited energy of the incident particles and the hit locations.

2.1 Front-end board

The front-end board amplifies and acquires the analog signal from the SSD. It consists of a packaged silicon strip sensor, two integrated charge measurement chips, and a signal processing circuit.

The SSD considered in this study was manufactured by Micron Semiconductor Ltd. (UK) [10]. The detector module has 128 alternating current coupling input channels, where the module dimensions are $97.30 \times 97.30 \text{ mm}^2$ with a $758\text{-}\mu\text{m}$ strip pitch and $96,968\text{-}\mu\text{m}$ strip length. The junction coupling capacitor is approximately 1000 pf for each channel at 10 kHz. When reverse voltage required for full depletion is provided, the thickness of the depletion layer is almost nearly the same as the sensor thickness, which is $300 \mu\text{m}$. The operating voltage is approximately 60 V with 10 nA as a typical leakage current. This packaged SSD is installed on the front-end board and is protected by an aluminum shielding box.

Considering the requirements of large readout channels and low noise, we adopted two VA140 application-specific integrated circuits (ASICs) to collect the charge. These are 64-channel charge measurement chips produced by IDEAS [11]. As Fig. 2 shows, each channel has a charge-sensitive preamplifier, a shaping circuit, as well as sample and hold circuits. During normal operation, charge signals from all input channels are amplified and held simultaneously.

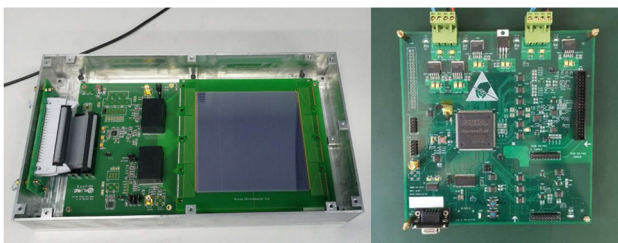


Fig. 1 (Color online) Front-end board together with SSD (left); data acquisition board (right)

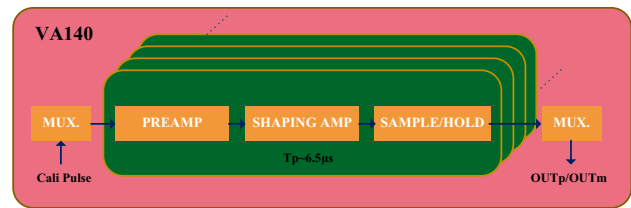


Fig. 2 (Color online) VA140 architecture

Then, the corresponding values are read out from the chip's multiplexer, which is controlled by a shift register. For noise cancellation, a differential current output pair (labeled as OUTp and OUTm in Fig. 2) is used. In addition, the VA140 chip also supports calibration measurements by injecting external charges.

2.2 DAQ board

The DAQ board has the functions of receiving commands from the host computer, digitizing the analog signal from the front-end board, providing bias voltage, and powering the whole system. This board mainly consists of an analog-to-digital converter (ADC) circuit, calibration circuit, high-voltage module, field programmable gate array (FPGA), and communication interface, as shown in Fig. 3.

This board uses an Intel Cyclone III FPGA clocked with a 20-MHz crystal oscillator. When the system is running and generating charge signals in the strip detector, the signals are amplified, shaped, and held by the VA140 chip. Differential analog signals are first converted to single-ended signals and then digitalized by a 3 MSPS ADC in the DAQ board. A digital-to-analog converter with an analog switch generates step pulses and then injects calibration charges into the front-end board through a 2-pF capacitance. The sensor's bias voltage is generated by a high-voltage module. Two types of communication interfaces are used in this board: a serial port with a 115,200-bps data rate for housekeeping data and a 1.5-Mbps universal serial bus together with a universal asynchronous receiver/transmitter interface for event data.

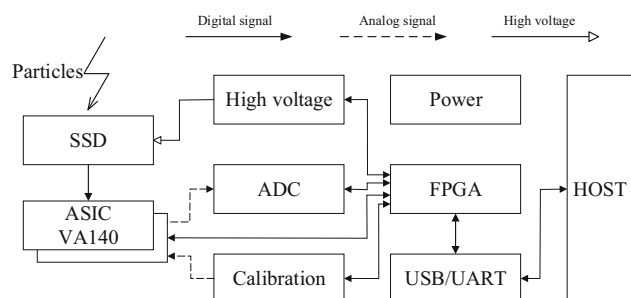


Fig. 3 SSD system block

Figure 4 is a timing diagram for a single event. Once the system is triggered, FPGA sends a hold signal to the VA140 chip. The delay between the trigger and hold signal is approximately 6.5 μs based on the ASIC shaping time. Two ASICs are daisy-chain connected, and the signals from all channels are shifted out sequentially with a 1.5-MHz clock. During 128 clock pulses, a 12-bit ADC is responsible for converting the analog signal into digital bits. All event data are simultaneously stored in the FPGA temporary memory and sent to the host computer. Typical dead time of this system is 1.9 ms.

3 TCT

TCT is used to study electric field properties and to characterize the charge collection of semiconductor devices. Two main factors make TCT a powerful tool for silicon detector study.

First, photons from a 1064-nm wavelength infrared laser possess energy greater than the silicon band gap (1.12 eV). The penetration depth for silicon is approximately 800 μm [12], which is deeper than the thickness of a common silicon detector. Moreover, when a focused laser beam hits the detector, the spot size of the beam, which is typically 11 μm at λ = 1064 nm, is much smaller than the detector strip pitch.

Second, the charge diffusion time is determined by the carrier mobility and electric field in the detector. In general, the diffusion time for holes and electrons are several tens of nanoseconds, and the shaping time of front-end electronics is usually much greater than the charge diffusion time for collecting charges.

In this study, we used a large scanning TCT apparatus introduced by a company named Particulars for SSD testing [13]. As shown in Fig. 5, the sensor was illuminated with a collimated pulsed infrared laser. Electron-hole pairs were generated inside the depleted bulk of the SSD, and the signal was processed by the DAQ board. Z-stage assistants

were used to find the focus point, and all strips in the silicon detector were scanned by moving the X-Y stage.

4 Experiment results

4.1 Linearity and electronic noise performance

We studied the linearity of the detector system using charge calibration and TCT laser irradiation. First, we evaluated all chip channels by injecting different voltage step pulses into the VA140 calibration pin through a 2-pF capacitor, as shown in Fig. 6a. The dynamic range was approximately 200 fC, but the linearity performance worsened when the input charge was greater than 180 fC. The chip became saturated when the input charge exceeded this value. All channels of the two ASICs displayed good linearity, and the average integral nonlinearity (INL) was less than 1.5%.

When the system linearity response was measured using a TCT laser beam, we selected one detector strip connected to channel 53 and allowed various laser intensities to be incident on the central area of this channel. The relative intensity of the laser was recorded by a laser module; results are shown in Fig. 6b. When the laser’s relative intensity was less than 42,000, the system showed a good linearity response with the INL of this measurement of better than 1.3%. However, this monitor module was neither aligned nor calibrated, and further testing will be conducted in the near future.

Root mean square (RMS) noise was tested both with and without the single SSD. Figure 6c shows that the average RMS noise was approximately 0.07 fC before the detector was assembled. When the detector was mounted, the equivalent input capacitance increased, and the average RMS noise in turn increased to 0.16 fC.

Fig. 4 Single-event readout sequence

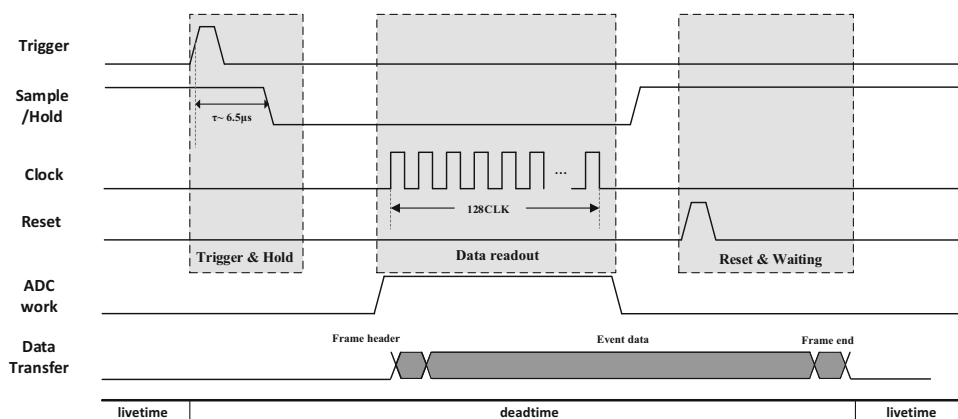


Fig. 5 Scheme of SSD testing system with a large scanning TCT apparatus

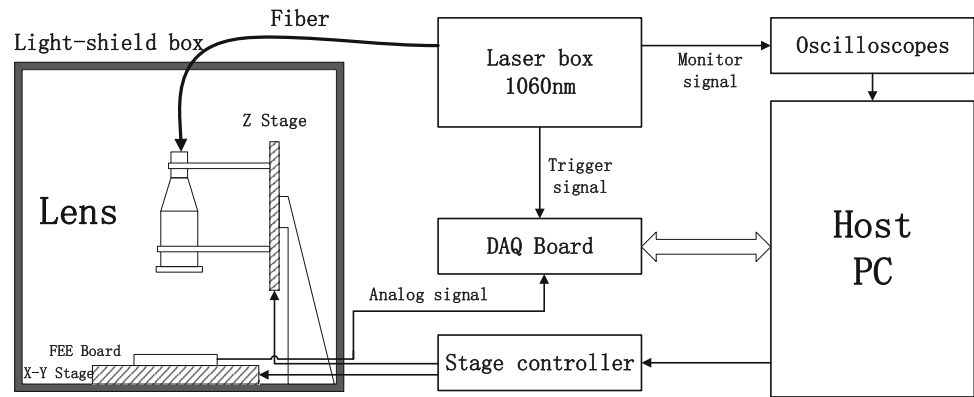
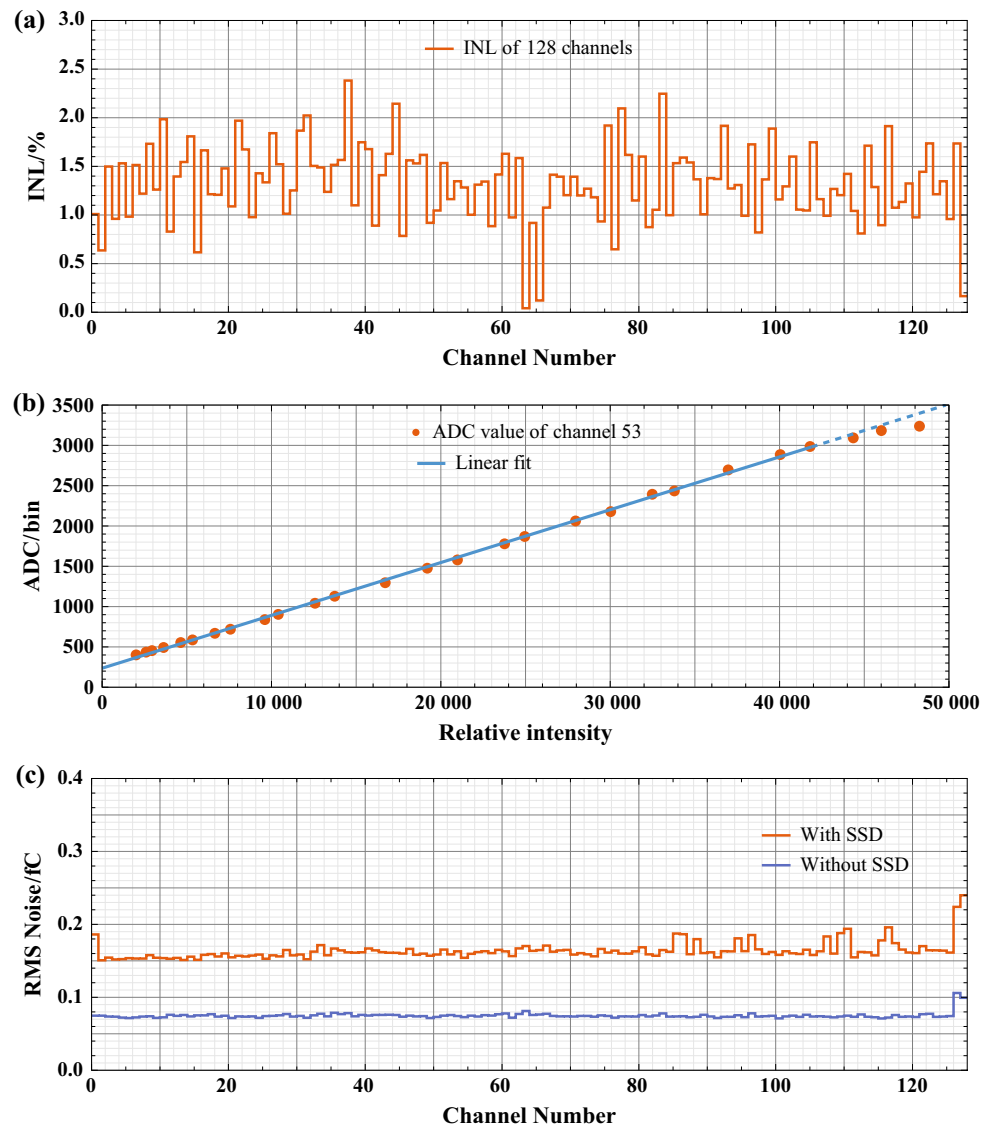


Fig. 6 **a** INL results from chip calibration with input charges from 0 to 200 fC. **b** Linearity response of the 53rd channel when measured with a TCT laser. **c** RMS noise of all input channels before and after the single SSD was mounted on the DAQ board



4.2 Strip scan and charge-sharing test

Traces of particles impacting the SSD can be determined by fired strips. In addition, charge sharing between

neighboring strips may improve spatial resolution. In this study, we used perpendicular laser scanning SSD to study charge distribution. Inside the light-shield box, a focused laser hit the detector strip while the X–Y stage moved in the

direction of the sensor strip. This achieved charge signals of 10 μm each along the moving stage path. We scanned all strips, where Fig. 7b shows the results for two neighboring strips.

Notably, we observed some zigzag results from Fig. 7b when the laser spot moved over the detector. Based on the SSD microstructure (Fig. 7a), each detector strip had eight narrow aluminum strips rather than one whole aluminum strip. When light hit the aluminum strips, a portion of the light was reflected and less energy was deposited in the detector. Therefore, eight local minimum ADC values can be seen in the scanned results.

When the laser spot moved into the gap between two adjacent detector strips, the induced charge signals collected in both strips. With the aid of TCT equipment, the division of charge between the strips could be measured

easily. Charge-sharing behavior can be represented by an η function [14]:

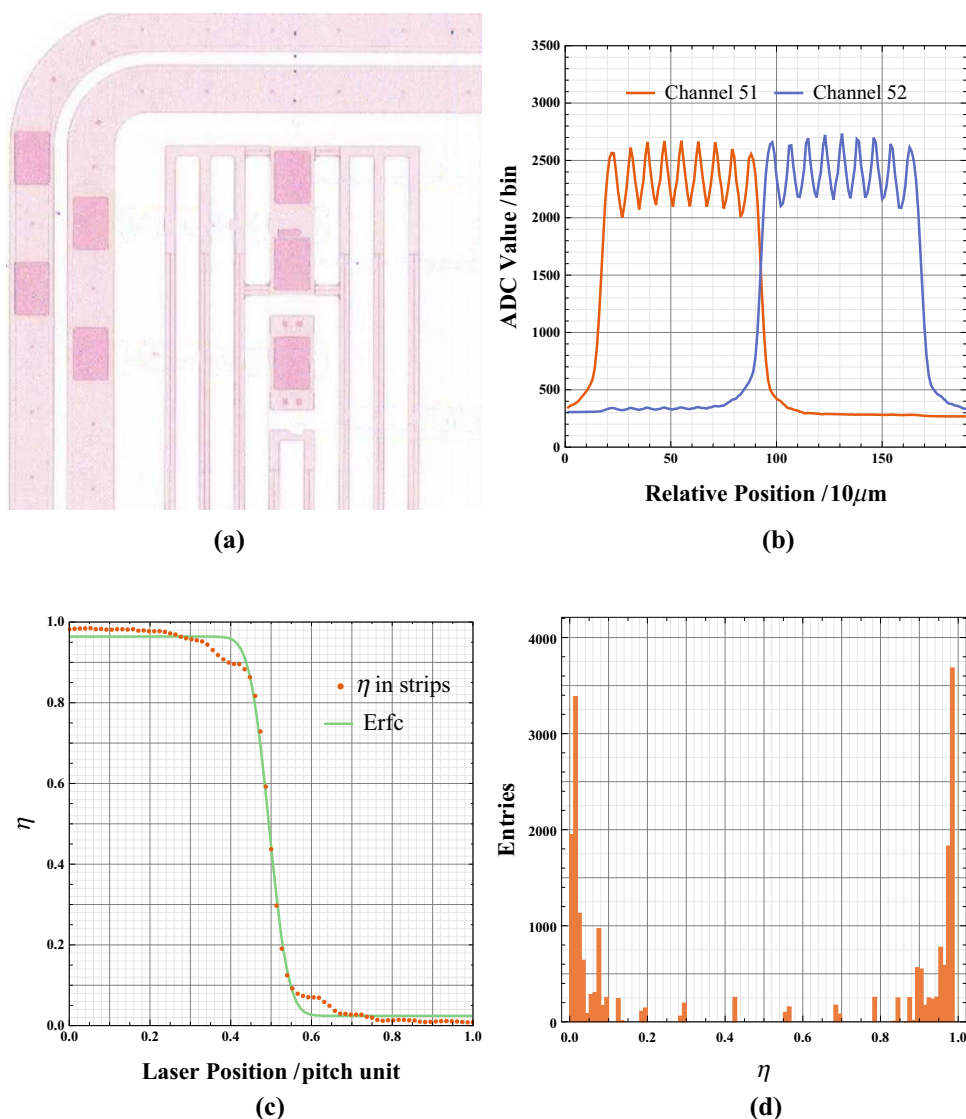
$$\eta_L(x_0) = \frac{Q_L(x_0)}{Q_L(x_0) + Q_R(x_0)}, \tag{1}$$

where x_0 is the laser spot coordinate measured relative to the left strip's central location, and Q_L and Q_R are the charges collected by the left and right strips, respectively. In addition, the x_0 coordinate can be normalized as:

$$u = \frac{x_0}{s}. \tag{2}$$

Here $s = 758 \mu\text{m}$ is the strip pitch. When $u = 0$, this means the laser position is in the center of the left strip, and $u = 1$ indicates the center of the right strip. Therefore, the η function can be written as:

Fig. 7 **a** Left top reign structure of the SSD. Bonding pads are present in the strip center, and a bias rail exists on the edge. **b** Scanning results of two strips, where a zigzag shape can be clearly seen. **c** η results measured by TCT equipment; the complementary error fitting function is also attached. **d** η value of hit events between two strips



$$\eta_L(u) = \frac{Q_L(u)}{Q_L(u) + Q_R(u)}. \quad (3)$$

In this test, photons were absorbed inside the sensor, and charges were deposited locally by the photoelectric effect. For perpendicular laser tracks, the charge was spread mainly by diffusion. The spatial extent of the charge cloud had an order of microns, which was far smaller than the strip pitch.

The η function result as shown in Fig. 7c revealed that when the laser beam was focused on the central area between the two strips ($u = 0.5$), they shared the charge signals equally. When the laser spot moved to the center of one of the strips ($u = 0$ at the left strip or $u = 1$ at the right strip), that strip collected nearly the entire charge. Because of the coupling capacitance between the two adjacent strips, the induced charge could not be collected in one strip even if the laser beam was located at the strip's center line.

Figure 7d shows that most of the events were located at $u = 0$ or $u = 1$, meaning that in the area between the two strips, most charge signals were collected by the strip closest to them rather than shared between the two strips.

The laser position in the pitch central area can be reconstructed by an inverse complementary error function. The relationship between the calculated and original

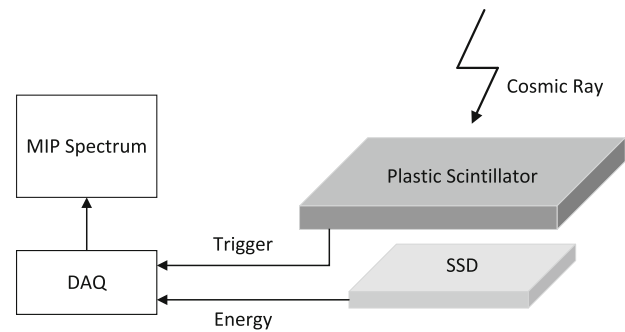


Fig. 9 Experimental setup of the cosmic ray spectrum test

positions is shown in Fig. 8a. In our test, the position resolution of the X - Y moving stage was approximately $1/8 \mu\text{m}$, whereas the laser moving step was $10 \mu\text{m}$. Therefore, the original laser position can be considered as the true position as compared with the reconstructed position.

Figure 8b shows the deviation distribution of the reconstructed position. The laser beam located at the position $930 \mu\text{m}$, which is the central point ($u = 0.5$) between the two strips, generated the best reconstruction results. The further the distance from the point $u = 0.5$, the larger was the reconstructed deviation. In this reconstruction area, the laser position deviations were less than

Fig. 8 a Reconstructed laser position vs. the original laser position. **b** Deviation distribution of the reconstructed laser position

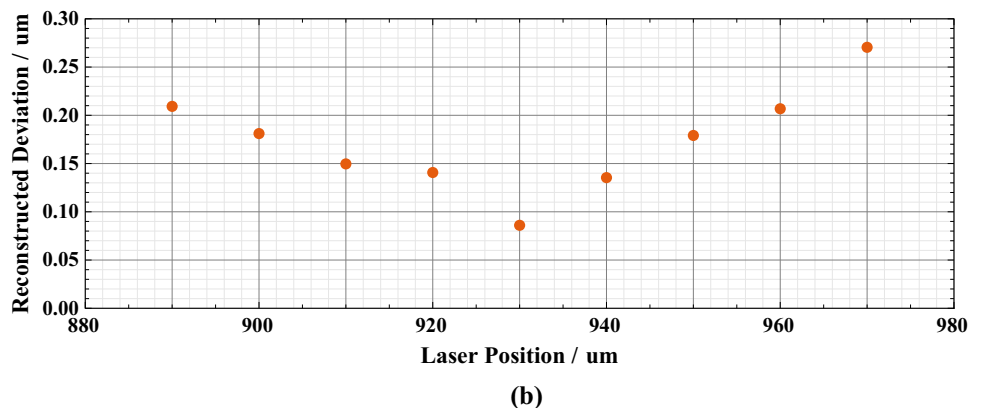
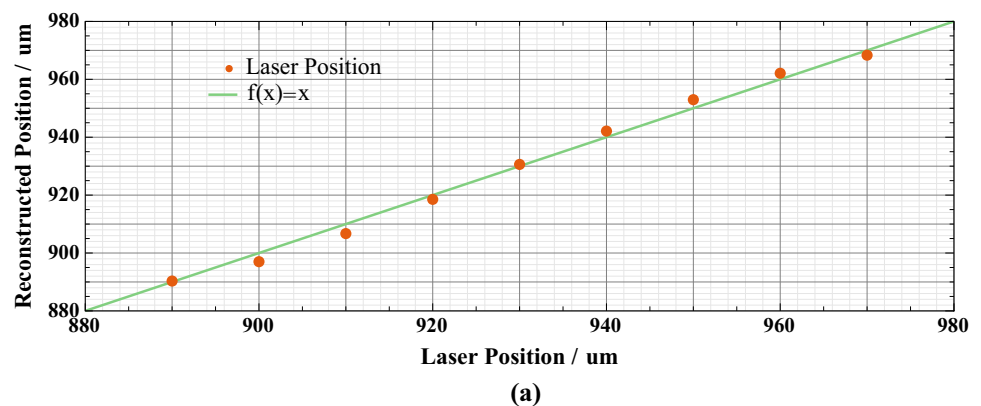
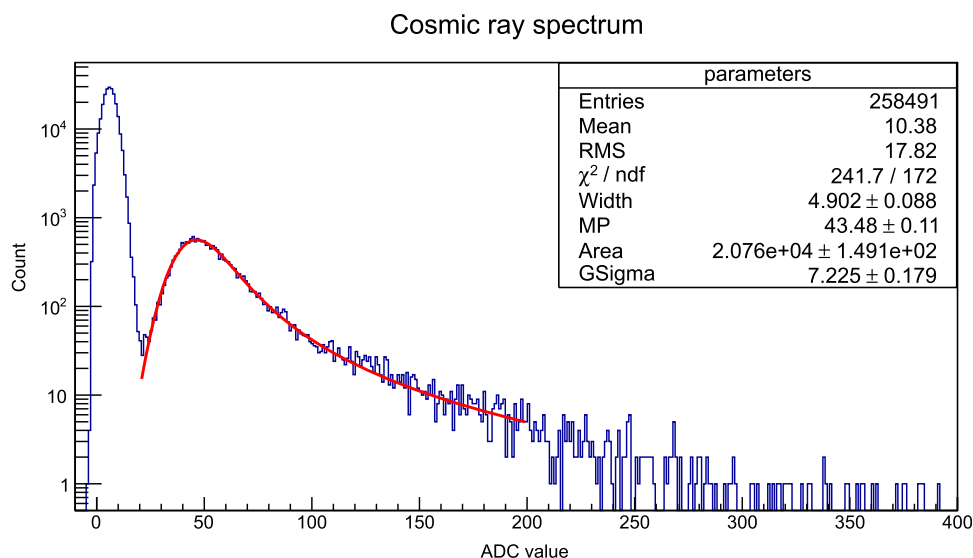


Fig. 10 Cosmic ray (MIP) spectrum fitted with convoluted Landau and Gaussian



0.27 μm , which means the detector response was pretty stable.

Please note that this position resolution was only in a small area (80 μm width) with respect to the strip pitch (758- μm width). When the laser beam location was close to the silicon strip, most charges are collected by a single strip, as shown in Fig. 7d.

4.3 Cosmic ray (MIP) spectrum

Cosmic ray muons interact with the detector mainly as minimum ionizing particles (MIPs), and the SSD system performance in our study was evaluated by a cosmic ray test. For this, we used a plastic scintillator as a trigger to detect the cosmic ray muons. The size of the scintillator detector was $15 \times 12 \text{ cm}^2$, which is bigger than the SSD module. The setup schematic is shown in Fig. 9.

The experiment lasted approximately 9 h, and the system pedestal was recorded every 2 h. High bias voltage and temperature were automatically monitored to ensure system safety. We obtained 258,491 trigger events, and the spectrum results are shown in Fig. 10.

Only one or two strips can be fired by a muon in single event, and in our study, the scintillator detector, which provided trigger signals, was larger than the SSD module. Therefore, most signals were baseline. After pedestal and common-mode noise were subtracted, these data formed a Gaussian distribution with an expectation value of 0 ADC.

One MIP will produce a most probable value of 22,000 $e^- h^+$ pairs in a 300- μm -thick silicon detector. This SSD system shows a gain of 14.5 bin/fC as calculated from a linearity test. Therefore, the MIP value collected by this system should ideally be approximately 50 bins (ADC). The MIP peak in this spectrum plot was fitted by

convoluted Landau and Gaussian functions, and the most probable parameter of Landau density was located at approximately 44 ADC. According to charge collecting efficiency, this value was reasonable.

5 Summary

The SSD system designed and discussed in this study featured a large dynamic range, low RMS noise, and a multi-channel readout. This detector can measure 128 strip channels simultaneously at a range of 180 fC with 0.16 fC RMS noise. Strip scanning based on TCT was shown to be efficient and precise. Based on this study's development of a miniature detector system, designing and studying a large SSD system in the future is possible.

References

1. A. Kounine, (AMS Collaboration), et al., The CMS experiment at the CERN LHC. *Int. J. Mod. Phys B* **12**, 1230005 (2012). <https://doi.org/10.1142/S0218301312300056>
2. G. Aad, (ATLAS Collaboration), et al., The ATLAS Experiment at the CERN Large Hadron Collider. *JINST* **3**(08), S08003 (2008). <https://doi.org/10.1088/1748-0221/3/08/S08003>
3. S. Chatrchyan, (CMS Collaboration), et al., The CMS experiment at the CERN LHC. *IEEE. JINST* **3**(08), S08004 (2008). <https://doi.org/10.1088/1748-0221/3/08/S08004>
4. W.B. Atwood, A.A. Abdo, M. Ackermann, et al., The large area telescope on the fermi gamma-ray space telescope mission. *Astrophys. J.* **697**(2), 1071 (2009). <https://doi.org/10.1088/0004-637X/697/2/1071>
5. J. Straver, O. Toker, P. Weilhammer et al., One micron spatial resolution with silicon strip detectors. *Nucl. Instrum. Methods. Phys. Res. Sect. A* **348**(2–3), 485 (1994). [https://doi.org/10.1016/0168-9002\(94\)90785-4](https://doi.org/10.1016/0168-9002(94)90785-4)

6. J. Chang, (DAMPE Collaboration), et al., The DArk matter particle explorer mission. *ASTROPART PHYS.* **95**, 6 (2017). <https://doi.org/10.1016/j.astropartphys.2017.08.005>
7. The CEPC Study Group, CEPC Conceptual Design Report: Volume 2—Physics and Detector [arXiv:1811.10545](https://arxiv.org/abs/1811.10545)
8. K. Gregor, Advanced Transient Current Technique Systems. *POSCI. Vertex* **2014**, 032 (2015). <https://doi.org/10.22323/1.227.0032>
9. S. Wang, J.H. Guo, Y. Zhang et al., High-resolution pixelated CdZnTe detector prototype system for solar hard X-ray imager. *Nucl. Sci. Tech.* **30**, 42 (2019). <https://doi.org/10.1007/s41365-019-0571-9>
10. Micron Semiconductor Ltd, Doubled Sided/AC Strip Detector. <http://www.micronsemiconductor.co.uk/strip-detectors-double-sided/>. Accessed 25 Apr 2019
11. IDEAS, The IDE1140 (previously VA140), <https://ideas.no/products/ide1140/>. Accessed 25 Apr 2019
12. G.F. Knoll, *Radiation Detection and Measurement*, 4th edn. (Wiley, Michigan, 2010), p. 52
13. Particulars advanced measurement systems. Products, 2014. Accessed 07 Apr 2018
14. O. Sokolvo, Prototyping of silicon strip detectors for the inner tracker of the ALICE experiment. *Ph.D. Thesis*, (University Utrecht, The Netherlands, 2006), p. 45